CLUSTERING OF ULTRALUMINOUS INFRARED GALAXIES IN THE BOÖTES FIELD

A Senior Scholars Thesis

by

ROBERTO DE ALBA

Submitted to the Office of Undergraduate Research
Texas A&M University
in partial fulfillment of the requirements for the designation as

UNDERGRADUATE RESEARCH SCHOLAR

April 2010

Major: Physics

CLUSTERING OF ULTRALUMINOUS INFRARED GALAXIES IN THE BOÖTES FIELD

A Senior Scholars Thesis

by

ROBERTO DE ALBA

Submitted to the Office of Undergraduate Research
Texas A&M University
in partial fulfillment of the requirements for the designation as

UNDERGRADUATE RESEARCH SCHOLAR

Approved by:

Research Advisor: Casey Papovich
Associate Dean for Undergraduate Research: Robert C. Webb

April 2010

Major: Physics

ABSTRACT

Clustering of Ultraluminous Infrared Galaxies
in the Boötes Field. (April 2009)

Roberto De Alba
Department of Physics and Astronomy
Texas A&M University

Research Advisor: Dr. Casey Papovich
Department of Physics and Astronomy

We study the nature and clustering of infrared (IR) galaxies at z~1.5-3 in a 9 deg^2 region from the Spitzer Deep, Wide-Field Survey (SDWFS) and the MIPS (Multiband Imaging Photometer for SIRTF) AGN (Active Galactic Nuclei) and Galaxy Evolution Survey (MAGES), taken at the Space Infrared Telescope Facility (SITRF). Using a method developed by Huang et al., we identify stellar-dominated IR-luminous galaxies at $1.5 < z < 3$ by selecting objects with characteristic infrared (3.6, 4.5, and 8.0 micron) flux ratios and 24 micron flux density (S(24) hereafter) > 0.3 mJy. We compute the angular correlation function of this sample over scales of 0.001 - 1 deg. Assuming an empirical redshift distribution, we derive spatial correlation scale lengths, $r_0 = 7.65 \pm 0.9\ h^{-1}$ Mpc for S(24) > 0.3 mJy and $8.73 \pm 2.1\ h^{-1}$ Mpc for S(24) > 0.5 mJy, with a possible scale length increase at higher 24 micron flux densities. We compare our sample to IR-luminous, dust-obscured galaxies (DOGs) at this redshift selected on the basis of their large mid-infrared to visible flux ratio, and which are known to include AGN, objects presumably powered by supermassive black hole accretion. While the DOG sample

includes objects with S(24) > 1 mJy, our IR-luminous, stellar-dominated sample contains few bright objects, and is approximately limited to S(24) <~ 0.6 mJy; high 24-micron brightness at z~2 requires a substantial amount of dust heated by AGN. At 0.3 mJy < S(24) < 0.6 mJy, the clustering strength of these two samples are nearly indistinguishable, and they are consistent with the clustering of other massive galaxies at these redshifts. Therefore, we conclude that these objects occupy dark-matter haloes of similar mass, on the order of $5 \times 10^{12} M_{\odot}$, and that these massive galaxies experience IR-active stages as a result both of star-formation and AGN activity with some duty cycle.

DEDICATION

This work is dedicated to Roberto De Alba, Jr. and Patricia De Alba, the parents of the author, for their unending support and encouragement of his love for science. I do not know where I would be without all of your motivation. No finite amount of thanks will ever suffice for all that you have done for me. I love you both.

ACKNOWLEDGMENTS

The author would like to thank his research advisor, Casey Papovich, for his guidance and support in research and the composition of the paper here presented. Thanks are also due to Steve and Keely Finkelstein for sharing their invaluable knowledge in the writing and debugging of the various types of computer programs necessitated by this work. Likewise, this project could not have been completed without the help of the MAGES team in acquiring their 24 micron flux measurements of galaxies in the Boötes field, which this work attempts to analyze. Ashby et al. also deserve much credit for the use of their data, made publicly available as the Spitzer Deep, Wide-Field Survey. The author would also like to express his gratitude towards Arjun Dey, Mark Brodwin, Christopher Kochanek, George and Marcia Rieke, Daniel Eisenstein, Benjamin Weiner, Emeric LeFloch, Michael Brown, Richard Cool, Lee Armus, Colin Borys, Mark Dickenson, Jane Morrison, Idit Zehavi, Daniel Stern, Herve Dole, Vandana Desai, Wiphu Rujopakarn, Miwa Block, David Herrera, and Buell Jannuzi. Lastly, I would like to thank Giselle Vazquez for her support and inspiration throughout this work.

Support for this work was provided by NASA through an award issued by JPL/Caltech.

TABLE OF CONTENTS

Page

ABSTRACT iii

DEDICATION v

ACKNOWLEDGMENTS vi

TABLE OF CONTENTS vii

LIST OF FIGURES viii

LIST OF TABLES ix

CHAPTER

I INTRODUCTION 1

Data sources 2
Infrared galaxy clustering 5
Connection to dark matter halos 5

II DATA REDUCTION AND THEORY 7

Galaxy matching 7
The angular correlation function 10
The bias factor 13

III RESULTS 16

Dark matter halo masses 19

IV SUMMARY AND CONCLUSIONS 23

REFERENCES 26

CONTACT INFORMATION 28

LIST OF FIGURES

FIGURE Page

1 The Boötes Constellation 4

2 Angular distribution of galaxies in the SDWFS catalogue 4

3 Offsets of matched sources between the SDWFS and MAGES data sets 9

4 A sample the galaxies meeting our selection criteria. 12

5 A reproduction of one of the random data sets created 12

6 Angular correlation functions of our galaxies in several flux density ranges 16

7 Correlation scale lengths of our galaxy clusters 17

8 Bias factor of our galaxies 18

9 Linear bias as a function of dark matter halo mass..... 20

10 Number distribution of galaxies in our sample compared to DOGs. 21

LIST OF TABLES

TABLE Page

1 Clustering of IR-Luminous Star Forming Galaxies in Boötes 19

CHAPTER I

INTRODUCTION

It appears that the majority of the stars in the universe formed at what we observe to be a redshift range of 1-3, or approximately 7.6-11.2 billion years ago. Much of this star formation occurs in galaxies that are very infrared luminous (they are *Ultraluminous* Infrared Galaxies), where we consider infrared wavelengths to be of the order 10-1000 microns. It has been shown that the star formation rate and infrared luminosity density of galaxies peak at these redshifts (Le Floc'h et al. 2009). This redshift range also coincides with high–quasar activity – or activity of galaxies with extremely Active Galactic Nuclei (AGN hereafter), likely resulting from emission processes associated with accretion onto supermassive black holes at the centers of the galaxies.

Although these Ultraluminous Infrared Galaxies and AGN are much more common in the distant universe, we do not yet understand how they are tied to the formation of large galaxies like the Milky Way. There is, however, knowledge to be gained from studying how these galaxies arrange themselves in space. This is because they are not distributed randomly, but instead cluster together. Studies of this sort are of interest to us because the amplitude of this clustering depends entirely on the mass and size of the dark matter halos in which these galaxies reside. Dark matter is an exotic and mysterious form of

---

This thesis follows the style of The Astrophysical Journal.

matter that interacts gravitationally but does not emit electromagnetic radiation at any wavelength, and, according to modern estimates, makes up more than 80% of all matter in the universe (Komatsu et al. 2008). And because dark matter interacts – rather strongly – only via gravitational forces, its distribution in space should not be uniform, but should display regions in which the local dark matter particles have coalesced as the universe evolved in time, in agreement with simulations (Springel et al. 2005). Thus, we can observe, through detailed studies of visible mass distributions, regions in space with dark matter over-densities (dark matter halos), and regions that are under-dense. In such studies, galaxies with large dark matter halos correspond to large clustering amplitudes.

The aim of the current research project is to use new methods for selecting ultraluminous infrared, star-forming galaxies from new data obtained using the Spitzer Space Telescope. We study the angular clustering of these galaxies, and implement mathematical tools – such as angular correlation functions, correlation scale lengths, and bias factors – to relate their distributions to those of the underlying dark matter structure and predict the masses of their dark matter halos. We then compare our results to those obtained previously for dust-obscured galaxies (DOGs) by Brodwin et al. (2008). By studying the clustering of ultraluminous galaxies in the distant Universe this way, we can directly link them to galaxies today.

Data sources

The data used in this project was obtained by the Spitzer Deep, Wide-Field Survey

(SDWFS), taken using the NASA's Spitzer Space Telescope (Werner et al. 2004), and covers a portion of the sky in the Boötes Constellation, displayed in Figure 1 (Ashby et al. 2009). It is one of the largest fields ever surveyed at such a large optical depth (corresponding to high redshift), covering approximately 9 deg^2 (about 36 times the angular size of the full moon). The data set itself is depicted in celestial coordinates in Figure 2. This survey, as its name suggests, also achieves significantly better sensitivity than prior surveys, allowing us to measure the infrared emission from galaxies that are further away than previously possible. These two factors allow us to gather a detailed and robust sample of galaxies, which is perfect for the project at hand.

SDWFS data was used primarily to obtain IRAC magnitudes for the galaxies in this field. The Infrared Array Camera (IRAC) onboard Spitzer allows for the measurement of data in the 3.6, 4.5, 5.8, and 8.0 micron bands (Fazio et al. 2004). These sources were then cross-correlated with data with data from the MIPS AGN & Galactic Evolution Survey (MAGES), which covers the same field as SDWFS, but in the far-infrared bands of 24, 70, and 160 microns (Jannuzi et al. 2010). The Multiband Imaging Photometer for SIRTF (MIPS), at the Space Infrared Telescope Facility (Rieke et al. 2004), is the instrument responsible for the precise measurements in these wavelength bands used here. We utilize the 24 micron band to find infrared-luminous galaxies. MAGES has an optical depth and field size comparable to SDWFS.

FIG. 1. – The Boötes Constellation.

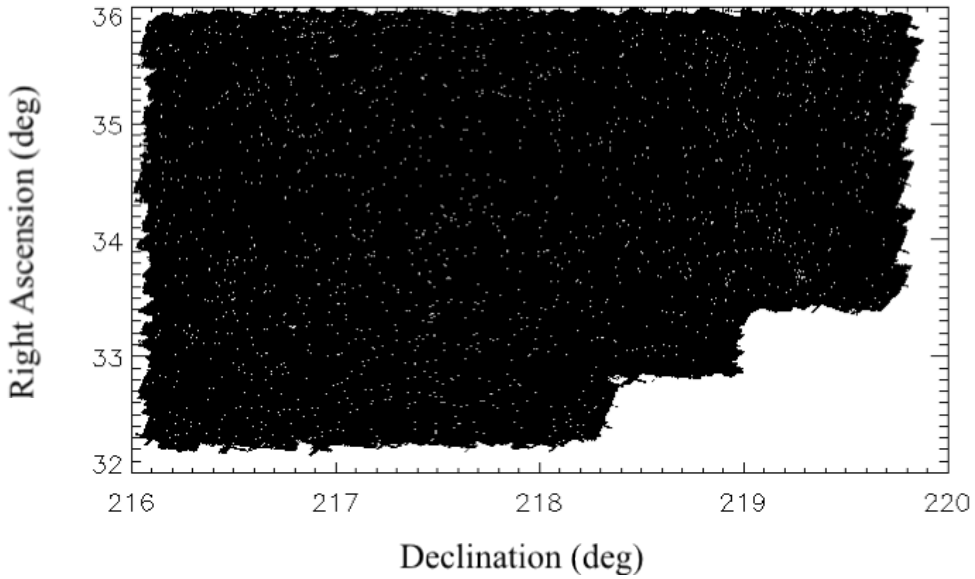

FIG. 2. – Angular distribution of galaxies in the SDWFS catalogue. (Each galaxy is represented by a single black point.)

Infrared galaxy clustering

To begin analyzing our galaxies, we need a straightforward, systematic method to select only star forming, ultraluminous infrared galaxies from our large data set. This is possible using a color selection technique recently proposed by Huang et al (2009). After obtaining the galaxies needed, they are sorted by infrared flux density. The clustering of these objects as compared to that of a completely random set of points in a field of the same angular size and shape is then computed using an estimator proposed by Landy & Szalay (1993). Henceforth, angular correlation functions are easily constructed for varying infrared brightness. Using these functions, we calculate correlation scale lengths, which are a measure of the amplitude of the clustering of these sources.

Connection to dark matter halos

In the cold dark matter (CDM) cosmological construction, the distribution of dark matter halos plays a vital role in the evolving structure of the universe. These halos, composed of dark matter particles that have coalesced through gravitational interactions over time, can be considered systems in quasi-equilibrium. According to CDM theory, most mass – and therefore ordinary matter – is tied to a dark matter halo. It is then obvious that knowledge of the clustering of galaxies can reveal to us information about the composition of their parent dark matter halos. More specifically, calculating what is commonly known as a cluster's bias factor, which compares over-densities in visible

matter to those in the local dark matter distribution, we then calculate the masses of their dark matter halos.

CHAPTER II

DATA REDUCTION AND THEORY

Galaxy matching

As noted above, two data surveys were used in this project: the Spitzer Deep, Wide-Field Survey (SDWFS) and the MIPS AGN and Galaxy Evolution Survey (MAGES). SDWFS is a four-epoch infrared survey of the Bootes field. It made use of the IRAC instrument on the Spitzer Space Telescope, and its resulting data is publicly available. The data includes four infrared bands and almost 700,000 sources, for a source density of ~70,000 galaxies/deg^2. The large survey time (200 hrs) is what gives this survey the depth needed to study objects beyond $z = 1.5$ and all the way to $z \approx 3$. Also, it is with this data that we can make use of the selection criteria put forth by Huang et al. (shown below).

$$0.05 < [3.6] - [4.5] < 0.4 \tag{2.1}$$

$$-0.7 < [3.6] - [8.0] < 0.5 \tag{2.2}$$

$$S(24) > 0.3 \ mJy \tag{2.3}$$

S(24), as mentioned previously, denotes the average flux density in the 24 micron band. Also, [3.6] represents the brightness magnitude in the 3.6 micron band, and is defined as

$$[3.6] = 23.9 - 2.5 \log\left(\frac{S(3.6)}{1 \ mJy}\right). \tag{2.4}$$

There are similar definitions for the remaining bracketed variables in Equations 2.1-2.

As described by Huang et al., Equations 2.1-3 can be used to select objects with $1.5 < z < 3.3$ because of a 1.6 micron stellar emission bump which moves into the 4.5 micron band at $z > 1.5$ and is a key factor in the color (2.1) given above. Similar features make the color (2.2) useful in selecting objects with $z < 3.3$. Because we select objects based on these features, we expect them to be dominated by stars and star formation.

The results for our galaxies are compared to those already obtained for dust-obscured galaxies (DOGs) by Brodwin et al. (2008). DOGs are selected based on a large difference between visible and mid-infrared magnitudes that arises because of the infrared emission of dust, and have been shown to contain AGN (Dey et al. 2008). The selection rule is

$$R - [24] > 14, \qquad (2.5)$$

where R is the visible red magnitude of these galaxies. Also, Brodwin et al. used a 24 micron flux density cutoff identical to ours (Equation 2.3) in their work.

In order to find corresponding galactic sources in both of these large sets, we have "matched" them using srcor, an IDL program distributed as part of the ASTROLIB package available on the Goddard Space Flight Center's NASA webpage. This program computes the "great circle" distance between two sources to determine regular distances on the celestial sphere. We used a critical radius of ~2 arcseconds for matching. Because it is expected that data points will not be located in exactly the same position

amongst the two data sets, a two-dimensional distribution was plotted of the offsets in their right ascension (RA) and declination (DEC) positions between the two sets, and the mean of this distribution was measured. This average offset was then reincorporated into the matching procedure as a bootstrap method to match the most possible sources and bring the mean offset closer to zero. The resulting distribution is displayed in Figure 3.

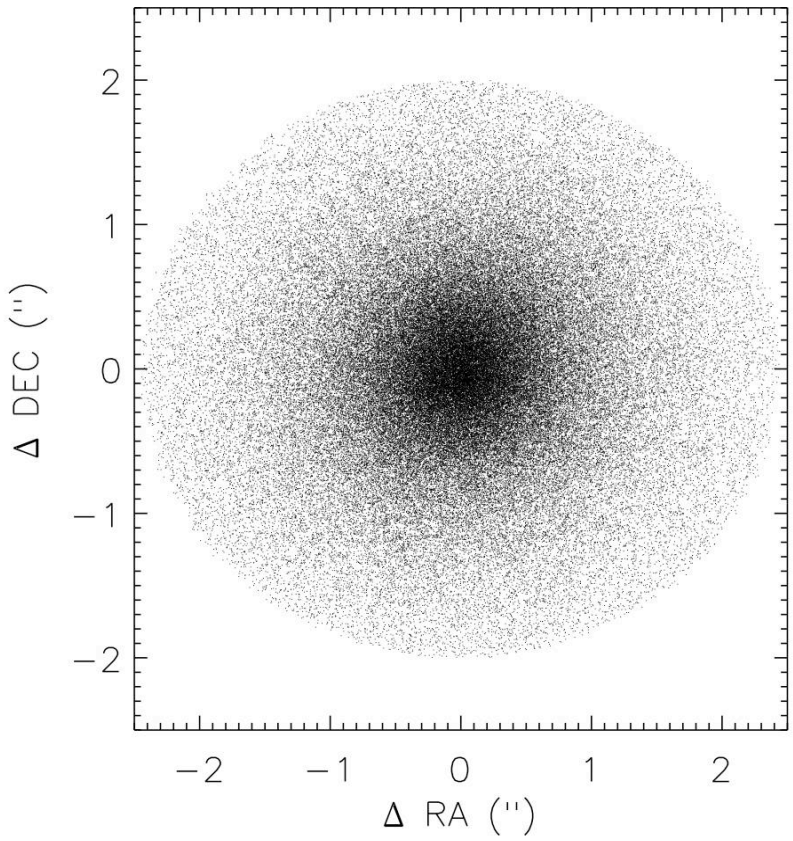

FIG. 3. – Offsets of matched sources between the SDWFS and MAGES data sets. Data points are measured in arcseconds and have a two-dimensional normal (Gaussian) distribution. We measure relative offsets from this distribution of $\langle \Delta RA \rangle = 0.0001'' \pm 0.002''$ and $\langle \Delta DEC \rangle = 0.0003'' \pm 0.002''$.

The angular correlation function

The angular correlation function, a two-point correlation function, is an effective means to calculate the angular clustering of an extragalactic source population from celestial coordinates (see: Peebles 1980). It involves counting the number of galaxy pairs in the data set as a function of separation angle and comparing this to the number of pairs in a randomly generated set of points with the same number density and in a field of the same geometry. Here we use the estimator for the angular correlation function of Landy and Szalay (1993), who showed that this estimator is more robust compared to other estimators. Their construction of the angular correlation function, which is widely considered the standard, is as follows:

$$w_{obs}(\theta) = \frac{DD(\theta) - 2DR(\theta) + RR(\theta)}{RR(\theta)}, \tag{2.6}$$

where $DD(\theta)$ is the number of data-data pairs in the angular separation $\left(\theta - \Delta\theta/2\ ,\ \theta + \Delta\theta/2\right)$, $RR(\theta)$ is the number of random-random pairs in the same interval, and $DR(\theta)$ corresponds to the number of data-random pairs. It is worth noting that we have not used a fixed value for $\Delta\theta$, but instead used angular separations that increased logarithmically. Weight maps, whose values are proportional to the observation time of each position in an observation field, provided for our data sets were used in order to create a random sample with a geometry identical to that occupied by our actual data. To decrease the variance associated with the randomness of this sample, we generated 1000 separate random data sets and summed their respective $RR(\theta)$ and $DR(\theta)$ values. We then normalized according to the relationship

$\Sigma_\theta RR(\theta) = \Sigma_\theta DR(\theta) = \Sigma_\theta DD(\theta)$. Samples of our true and random data sets can be seen in Figures 4 & 5. Usually the angular correlation function is parameterized as a power-law of the form

$$w(\theta) = A_w \theta^{-\beta}. \tag{2.7}$$

After computing this function in its discrete form (Equation 2.6), we find the best fit of our resulting data to the above power-law and calculate values for A_w and β, the amplitude and scaling exponent of our function.

Because so far we have only considered angular clustering, in which our galaxies have been compressed into our two-dimensional plane of view, we now move forward to consider the full three-dimensional spatial clustering of our galaxies. Like the angular correlation function given in Equation 2.7, the spatial correlation function has a power-law form and is written as

$$\xi(r) = \left(\frac{r}{r_0}\right)^{-\gamma}, \tag{2.8}$$

where $\gamma = \beta + 1$ and r_0 is commonly referred to as the spatial correlation scale length. The angular correlation function is related to spatial correlation function by the Limber projection (Magliocchetti & Maddox 1999),

$$A_w = \frac{H_\gamma r_0 \int F(z) r_c^{1-\gamma}(z) N^2(z) E(z) dz}{(c/H_0)\left[\int N(z) dz\right]^2}, \tag{2.9}$$

where $r_c(z)$ is the commoving radial distance, which can be found in Hogg (2000), $N(z)$ is the redshift distribution, here assumed to be a Gaussian centered at $z = 1.96$ (Huang et

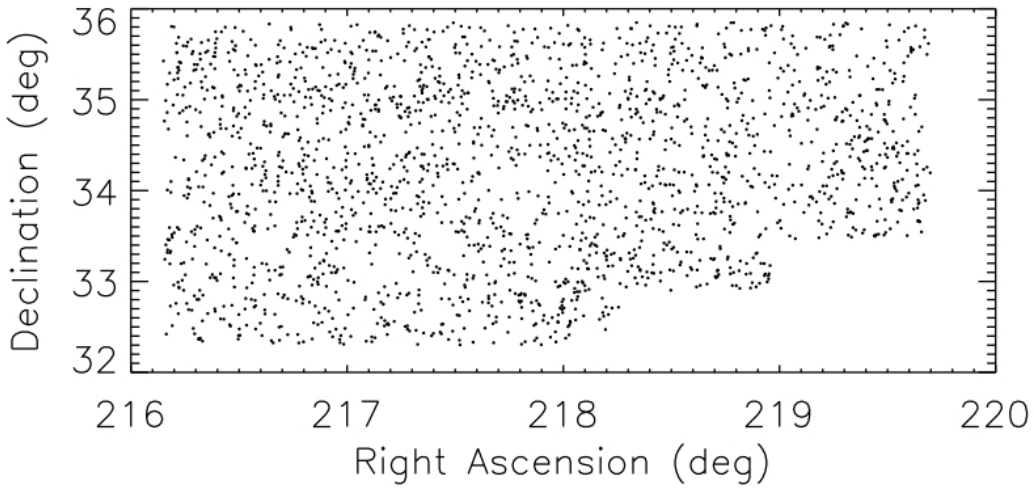

FIG. 4. – A sample the galaxies meeting our selection criteria. They are star forming, infrared luminous galaxies with $1.5 < z < 3.3$, and are used in measuring $DD(\theta)$. These galaxies show clear regions of excesses clustered together and voids.

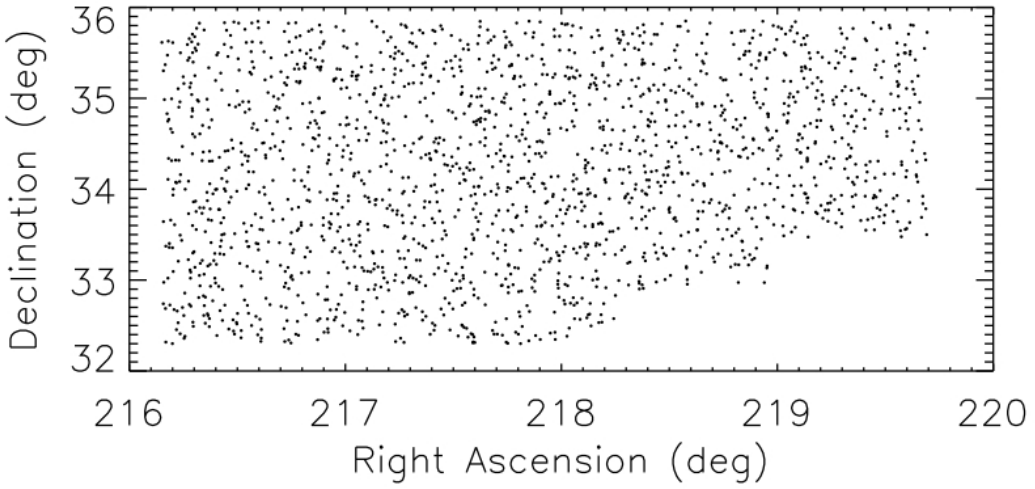

FIG. 5. – A reproduction of one of the random data sets created. Data sets such as this were used in measuring $RR(\theta)$ and $DR(\theta)$. Notice that the number density of these sources is similar to that of our actual galaxies displayed in Figure 4. Note also the similar geometries of these fields.

al. 2009), and H_γ, $E(z)$ are described by:

$$H_\gamma = \Gamma\left(\frac{1}{2}\right)\frac{\Gamma\left[(\gamma-1)/2\right]}{\Gamma(\gamma/2)}, \tag{2.10}$$

$$E(z) = \sqrt{\Omega_m(1+z)^3 + \Omega_\Lambda} \tag{2.11}$$

(Quadri et al. 2007). $F(z)$ in Equation 2.9 is the function describing the evolution of clustering with redshift, taken as $F(z) = (1+z)^{-(3-\gamma+\varepsilon)}$, where ε is a parameter which is usually taken to be $\varepsilon = \gamma - 3$ for constant clustering, $\varepsilon = 0$ for stable clustering, and $\varepsilon = \gamma - 1$ for stable growth (Quadri et al. 2007). As usual, c denotes the speed of light, H_0 is the present day value for Hubble's constant (the numerical factor that sets the speed with which the universe is expanding), Γ represents ordinary gamma functions, and Ω_m, Ω_Λ represent the matter density and dark energy density of the universe, respectively.

The bias factor

When attempting to extract information about dark matter halos from galaxy clustering studies, one invariably encounters a parameter commonly referred to as the bias factor. This number relates the clustering of dark matter halos to that of ordinary matter in the given field of study. It can be written as:

$$b = \frac{\sigma_{8,gal}}{\sigma_8(z)}, \tag{2.12}$$

where $\sigma_8(z)$ is the variance in $8\,h^{-1}$Mpc spheres of space (Quadri et al. 2007) and is calculated according to the relationship

$$\sigma(M,z) = D(z)\sigma(M,0). \tag{2.13}$$

In the preceding equation, $D(z)$ represents the growth factor of linear matter fluctuations and gives the variance its evolution with redshift, (Carroll et al. 1992). It is given by

$$D(z) = \frac{g(z)}{g(0)(1+z)}, \tag{2.14}$$

in which

$$g(z) \cong \frac{5}{2}\Omega_m(z)\left[\Omega_m{}^{4/7}(z) - \Omega_\Lambda(z) + \left(1+\frac{\Omega_m(z)}{2}\right)\left(1+\frac{\Omega_\Lambda(z)}{70}\right)\right]. \tag{2.15}$$

The factor $\sigma(M,0)$ in Equation 2.13 is the variance at $z=0$ and is calculated using

$$\sigma_M{}^2 = \frac{1}{2\pi^2}\int_0^\infty dk\, k^2 P(k) W^2(kR) \tag{2.16}$$

(Mo & White 2002), where

$$P(k) \propto k \times \frac{\ln(1+2.34q)}{2.34q} \times \left[1+3.89q+(16.1q)^2+(5.46q)^3+(6.71q)^4\right]^{-1/4}, \tag{2.17}$$

$$q = \frac{k}{\Omega_m\, h^2 Mpc^{-1}} \tag{2.18}$$

and

$$W(kR) = \frac{3(\sin kR - kR\cos kR)}{(kR)^3}. \tag{2.19}$$

To find the constant of proportionality in Equation 2.17, we make use of the condition $\sigma_{8h^{-1}Mpc} = 0.9$.

The final remaining factor in Equation 2.12, $\sigma_{8,gal}$, is found by calculating the variance of the spatial galaxy distribution, $\xi(r)$ (Equation 2.8), and takes the form

$$\sigma_{8,gal} = \sqrt{\frac{72}{(3-\gamma)(4-\gamma)(6-\gamma)2^{\gamma}}\left(\frac{r_0}{8h^{-1}Mpc}\right)^{\gamma}} \tag{2.20}$$

(Quadri et al. 2007). The factor R in Equation 2.16 is the radius of the spheres in which the variance is being measured. As mentioned previously, here we use $R = 8\ h^{-1}Mpc$ to compute the bias of our galaxies. Later, we will use the mean mass density of the universe to couple R to the mass within each given sphere and thus be able to directly relate bias to halo mass.

Once we have successfully calculated the bias factor for our sample, we can analytically compute the evolution of this factor with redshift in order to gain an understanding of the type of galaxies our sources would correspond to at the current epoch, i.e. $z = 0$. We track the evolution of the bias factor according to the equation

$$b(z) = 1 + \frac{b(0) - 1}{D(z)}, \tag{2.21}$$

in which $D(z)$ is the same growth factor given before and $b(0)$ represents the value of the bias at $z = 0$ and can be adjusted until the function intersects the bias of our sample at higher redshifts. Thus we have shown that this factor not only enables us to calculate values for the masses of the dark matter halos our galaxies are in, but it also helps us predict the types of galaxies they would evolve to at present day.

CHAPTER III

RESULTS

The angular correlation functions of our galaxies were computed using the estimator proposed by Landy & Szalay described previously (Equation 2.6) for several different flux density bins. The angular correlation functions for our sample are shown in Figure 6. Each plot displays significant and distinct clustering that supersedes purely random

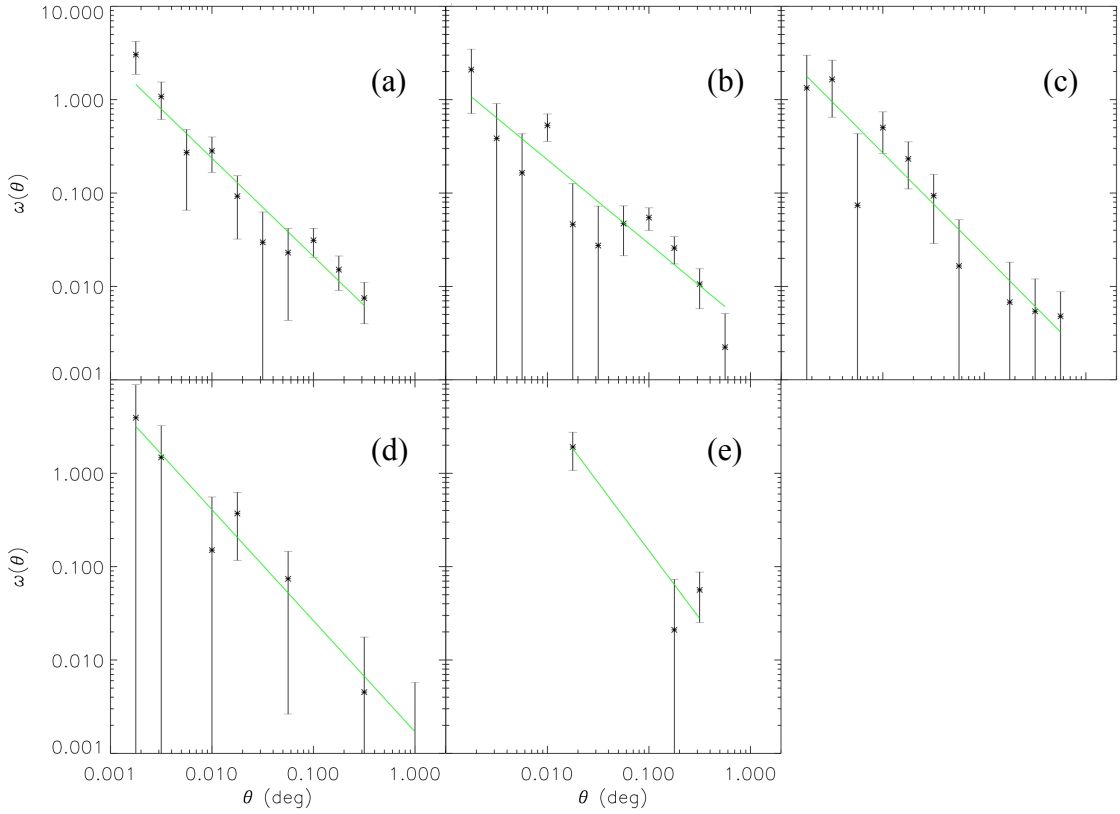

FIG. 6. – Angular correlation functions of our galaxies in several flux density ranges. Correlation functions are plotted for:
(a) all sources, (b) $0.3 \le F_{24}(mJy) < 0.5$, (c) $F_{24}(mJy) > 0.4$,
(d) $F_{24}(mJy) > 0.5$, and (e) $F_{24}(mJy) > 0.6$.

organization. Fewer sources at higher 24 micron flux densities leads to larger uncertainties. Best-fit functions (green lines) are used to compute correlation scale lengths in the manner described by Equations 2.9-11.

The next task was to use the parameters from the best-fit functions of our angular correlation functions to compute correlation scale lengths (shown in Figure 7 in comparison to those of dust-obscured galaxies from Brodwin et al. 2008). These ranged from 7.65 ± 0.92 h^{-1}Mpc for $F_{24} > 0.3$ mJy and 18.0 ± 4.9 h^{-1}Mpc for $F_{24} > 0.6$ mJy,

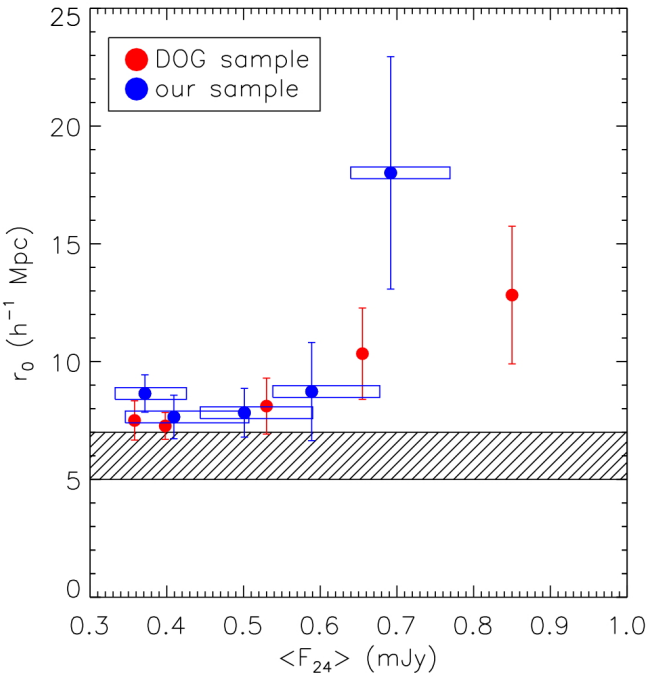

FIG. 7. – Correlation scale lengths of our galaxy clusters (as compared to those of DOGs). The scale lengths of our galaxies are indistinguishable from those of DOGs at low flux densities. The striped region depicts typical scale lengths for galaxies with $M^*>3x10^{10}$ $M_\odot$ at $2<z<3.5$. Blue boxes enclose 50% of our galaxies in a given 24 micron flux density range.

where, once again, the large uncertainty is due mostly to a decrease in the number of data points. Our stellar-dominated, IR-luminous galaxies have correlation scale lengths that are indistinguishable from those of dust-obscured galaxies at low flux densities, which suggests that these objects occupy dark matter halos of similar masses. We see a possible scale length increase at $F_{24} >\sim 0.7$ mJy, suggesting that as our galaxies increase in 24 micron flux density they become more strongly clustered. DOGs are shown to reach much higher flux densities.

Once the correlation scale lengths were computed, it was then possible to compute the bias factors of our sources. Bias factors are plotted as functions of redshift in Figure 8.

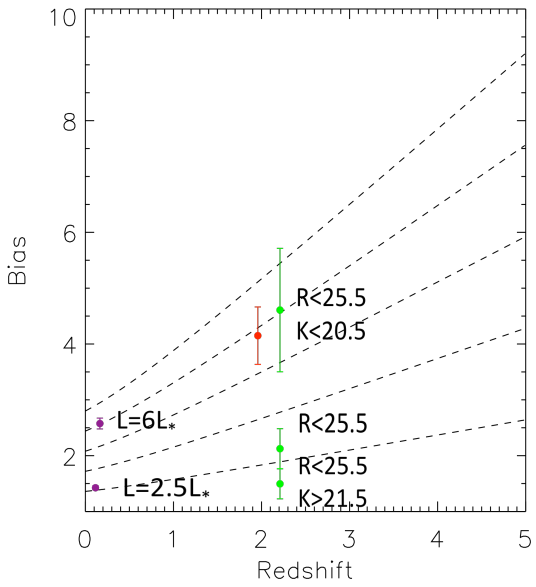

FIG. 8. – Bias factor of our galaxies (displayed in red). Purple points are relatively nearer galaxies (Zehavi et al. 2005). Green points are z~2 galaxies with AB magnitude R < 25.5 (Adelberger et al. 2005; see also Quadri et al. 2007). We see that at $z = 0$ our galaxies correspond to a bias of ~2.5, meaning luminosities around $6\,L_*$.

TABLE 1
CLUSTERING OF IR-LUMINOUS STAR FORMING GALAXIES IN BOÖTES

$S_{24}(mJy)$	$\langle S_{24} \rangle (mJy)$	N	$r_0(h^{-1}Mpc)$	b	Halo Mass $\log(M / M_{\odot})$
>0.3	0.4459	2233	7.65±0.92	4.15±0.51	12.7±0.2
0.3-0.5	0.3816	1635	8.65±0.79	4.32±0.38	12.8±0.1
>0.4	0.5347	1185	7.83±1.03	4.35±0.60	12.8±0.2
>0.5	0.6218	598	8.73±2.08	5.20±1.36	$13.0^{+0.3}_{-0.4}$
>0.6	0.719	263	18.0±4.9	16.0±5.4	$14.1^{+0.3}_{-0.4}$

Notes: S_{24} refers to 24 micron flux density, N denotes the number of galaxies in each bin, and b is the bias factor.

The dashed curves show the analytical evolution of bias with redshift according to Equation 2.21. Our data, computed by Equation 2.12, is displayed in red for all sources. For our sample, bias seems to be independent of 24 micron flux density at low fluxes, and so other flux bins are not shown. Individual bias values, along with all other relevant parameters, can be found in Table 1. Following the tracks in Figure 8, we see that at redshift zero our galaxies correspond to objects with bias around 2.5. This value corresponds to galaxies with luminosities around $6\,L_*$, where L_* is a characteristic galaxy luminosity and the Milky Way approximately a $1\,L_*$ galaxy.

Dark matter halo masses

We can relate the bias factor to the masses of the dark matter halos occupied by our galaxies by writing it as a function of this mass. A bias of this functional form was originally proposed by Sheth et al. (2001). We thus write the linear halo bias as

$$b_h = 1 + \frac{1}{\delta_c}\left[\nu'^2 + b\nu'^{2(1-c)} - \frac{\nu'^{2c}/\sqrt{a}}{\nu'^{2c} + b(1-c)(1-c/2)}\right], \qquad (3.1)$$

where $\nu' = \sqrt{a}\delta_c / \sigma(M,z)$, $\delta_c \approx 1.69$, $a = 0.707$, $b = 0.5$, and $c = 0.6$. $\sigma(M,z)$ is the same variance function described in Equations 2.13-16. However, here we relate R to the mass in the region as mentioned previously by using the mean mass density of the universe at a give redshift. Using the value which appears in Carroll & Ostlie (2007), $\bar{\rho}_m = 2.56 \times 10^{-27} kg\, m^{-3}$, we tie the radius of a given sphere in which we wish to compute the variance to the mass of the dark matter contained within through the relationship $M = \frac{4}{3}\pi R^3 \bar{\rho}_m$. We have plotted Equation 3.1 in Figure 9. Utilizing the galaxy biases computed through Equation 2.12, we can graphically compare these calculated values to the function plotted and read off the corresponding halo mass.

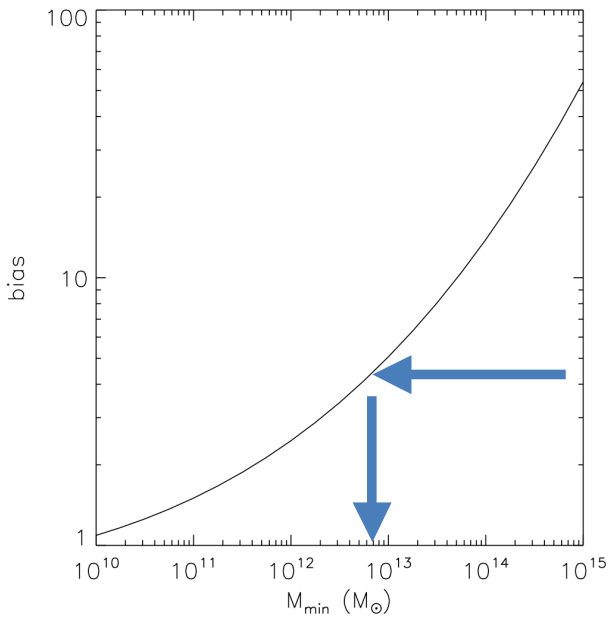

FIG. 9. – Linear bias as a function of dark matter halo mass. We can estimate the halo mass by finding the value corresponding to the bias calculated for our data set. Based on the bias found for our galaxies, we see that their dark matter halos have masses of $\sim 5 \times 10^{12} M_\odot$.

Using this method, we see that our galaxies reside in dark matter halos of mass approximately 1.5×10^{13} $M_{\odot}$. This is larger than value found for DOGs in the same field by Brodwin et al., which is 1.6×10^{12} $M_{\odot}$, by an order of magnitude.

Finally, we can compare the number distribution of galaxy sources in our sample at different 24 micron flux densities to the DOGs. A histogram of these two data sets is plotted in Figure 10. At low flux densities, these galaxies are present in approximately equal number. The DOGs dominate the number distribution at high 24 micron flux

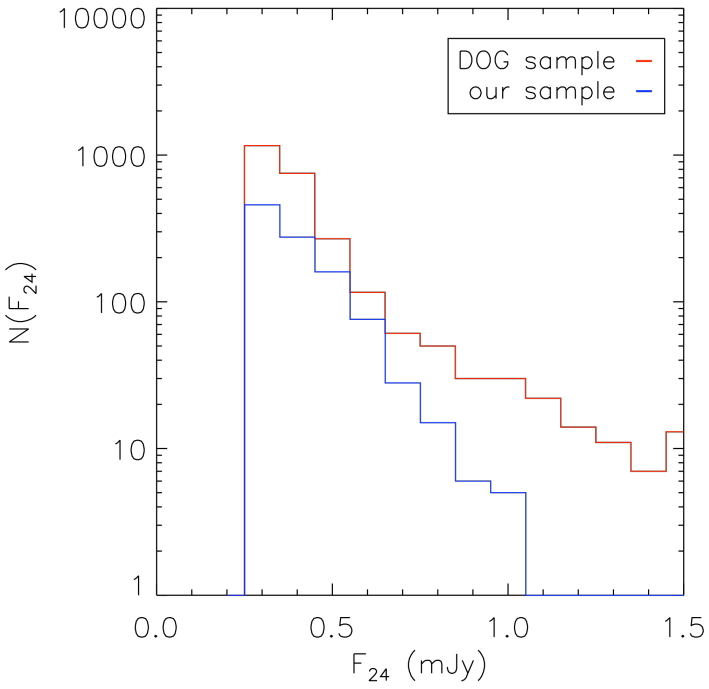

FIG. 10. – Number distribution of galaxies in our sample compared to DOGs. Both sets of galaxies reside in the same field. DOGs are shown to reach much higher infrared flux densities than our sources, suggesting that AGN are needed to reach such high emission.

densities, suggesting that AGN are needed to reach such high emission. This is consistent with conclusions drawn from DOG-selected samples (Dey et al. 2008). However, we find that our infrared-luminous, star forming galaxies and DOGs have similar clustering strengths (Figure 7). Therefore, both our sample and DOGs reside in similar dark matter halos. This implies that galaxies in dark matter halos of $M \sim 5 \times 10^{12} M_{\odot}$ at $z \sim 2$ include both star forming and AGN powered infrared-luminous galaxies.

CHAPTER IV

SUMMARY AND CONCLUSIONS

We have used flux-density ratios measured at 3.6, 4.0, and 8.0 microns and 24 micron flux density in the Boötes constellation from data obtained by the SDWFS and MAGES teams to select infrared-luminous galaxies in the redshift range $1.5 < z < 3.3$. In total, 2,233 galaxies met all of our criteria. We measured a spatial clustering correlation scale length of $7.65 \pm 0.92\, h^{-1} Mpc$ for these sources. This proved to be consistent with DOGs (selected based on Equations 2.3 and 2.5) at this redshift selected on the basis of high infrared-to-optical flux ratios, implying that at their dark matter halos are indistinguishable from our infrared-luminous, star forming galaxies at infrared flux densities around $\sim 0.4\, mJy$. This correspondence holds true as the mean flux density increases to $\sim 0.6\, mJy$. As we move to higher flux densities, however, both our sources and DOGs display a significant growth in scale length, and we begin to see a possible divergence between the correlation scale lengths, and hence dark matter halo masses, of these two classes of galaxies. Given the large error associated with our data at the higher 24 micron flux densities, though, it is very possible that our galaxies and DOGs do still occupy the same dark matter halos. We find dark matter halo masses of $\sim 5.0 \times 10^{12} M_{\odot}$ for galaxies with S(24) > $0.3\, mJy$ and $\sim 1.3 \times 10^{14} M_{\odot}$ for S(24) > $0.6\, mJy$ galaxies, which are close to the values obtained for DOGs by Brodwin et al. (2008): $\sim 1.5 \times 10^{12}$ $M_{\odot}$ and $\sim 1.0 \times 10^{13} M_{\odot}$. This leads us to conclude that galaxy clusters in dark matter halos of this mass range contain both star-forming galaxies and AGN.

We computed biases for our infrared-luminous, star forming galaxies of 4.15±0.51 and 16.0±5.4 for S(24) > 0.3 mJy sources and S(24) > 0.6 mJy sources, respectively. Biases remain approximately constant at low fluxes densities, but at large flux densities (S(24)>~ 0.6 mJy) we see a rapid increase, leading to much larger luminosities (and halo masses) at present day. Interestingly, such a large increase in bias is not seen in DOGs. Brodwin et al. find a bias of $5.33^{+1.65}_{-1.04}$ for galaxies in the high flux density range, which differs from our value by a factor of 3. The large bias found for our galaxies is likely partially accountable to the relatively small number of sources at this flux density. Because the luminosities of our galaxies are dominated by star formation and not AGN, as in DOGs, they are typically much dimmer, leading to lower visibility from our vantage point. Detecting such a small number of galaxies in this admittedly large field, we measure an overabundance of galaxies within ~0.01 deg of each other, leading to a large bias and dark matter halo mass, as well as large errors. Extrapolating our data to present day, we show in Figure 8 that our sources would have a bias around 2.5 at $z = 0$, which corresponds to galaxies with luminosities of ~6 L_*, or approximately 6 times brighter than the Milky Way.

After comparing the number distribution of our star-forming galaxies to that of DOGs in our field, we showed in Figure 9 that these two sets have an almost identical number of sources at low flux densities. At ~0.7 mJy, we begin to see a growing discrepancy between the number of sources in these two data sets, and at ~1.1 mJy the only sources remaining are DOGs. Both of these traits are attributed to AGN activity within the

DOGs that is not present in our galaxies. This agrees with conclusions of Pope et al. (2008) that although DOGs are a mixed population of starbursts (i.e. star forming galaxies) and AGN, they are dominated mostly by star formation. It is thus apparent that there is significant overlap between our galaxies and DOGs at low flux densities. This fact, along with the similar values computed for their biases and dark matter halo masses, leads us to conclude that our star forming galaxies and DOGs do in fact occupy nearly identical dark matter halos. This parallel seems to hold true through our entire flux density range. At low flux densities, they both show significant clustering. However, in the high flux density limit, both galaxy classes exhibit even stronger clustering, implying that these bright sources live in much richer galactic neighborhoods than do the dimmer sources.

REFERENCES

Adelberger, Kurt L., Erb, D. K., Petttini, M., Reddy, N. A., Shapely, A. E., & Steidel, C. S. 2005, Astrophysical Journal, 620, L75

Ashby, M. L. N., Stern, D., Brodwin, M., Griffith, R., & Eisenhardt, P. et al 2009, 701, 428

Brodwin, Mark, Dey, A., Brown, M. J. I., Pope, A., & Armus, L. et al. 2008, Astrophysical Journal, 687, L65

Carroll, Bradley W., & Ostlie, D. A. 2007, An Introduction to Modern Astrophysics, 2nd ed. (San Francisco: Addison-Wesley)

Carroll, Sean M., Press, W. H., & Turner, E. L. 1992, Annual Review of Astronomy and Astrophysics, 30, 499

Dey, Arjun, Soifer, B. T., Desai, V., Brand, K., & Le Floc'h, E. et al. 2008, Astrophysical Journal, 677, 943

Fazio, G. G., Hora, J. L., Allen, L. E., Ashby, M. L. N., & Barmby, P. et al. 2004, Astrophysical Journal Supplement Series, 154, 10

Hogg, David W. 2000, arXiv:astro-ph/9905116

Huang, J.-S., Faber, S. M., Daddi, E., Laird, E. S., & Lai, K. et al. 2009, Astrophysical Journal, 700, 183

Jannuzi, Buell, Weiner, B., Block, M., Borys, C., & Eisenstein, D. et al. 2010, Bulletin of the American Astronomical Society, 41, 513

Komatsu, E., Dunkley, J., Nolta, M. R., Bennett, C. L., & Gold, B. et al, 2009 Astrophysical Journal Supplement Series, 180, 330

Landy, Stephen D., & Szalay, A. S. 1993, Astrophysical Journal, 412, 64

Le Floc'h, Emeric, Aussel, H., Ilbert, O., Riguccini, L., & Frayer, D. T. et al. 2009, Astrophysical Journal, 703, 222

Magliocchetti, M., & Maddox, S. J. 1999, Monthly Notices of the Royal Astronomical Society, 306, 988

Mo., H. J., & White, S. D. M. 2002, Monthly Notices of the Royal Astronomical Society, 336, 112

Peebles, P. J. E. 1980, The Large-Scale Structure of the Universe (Princeton: Princeton Univ. Press)

Pope, Alexandra, Chary, R.-R., Alexander, D. M., Armus, L., & Dickinson, M. et al. 2008, Astrophysical Journal, 675, 1171

Quadri, Ryan, van Dokkum, P., Gawiser, E., Franx, M., & Marchesini, D. et al. 2007, Astrophysical Journal, 654, 138

Rieke, G. H., Young, E. T., Engelbracht, C. W., Kelly, D. M., & Low, F. J. et al. 2004, Astrophysical Journal Supplement Series, 154, 25

Springel, Volker, White, S. D. M., Jenkins, A., Frenk, C. S., & Yoshida, N. et al. 2005, Nature, 435, 629

Werner, M. W., Roellig, T. L., Low, F. J., Rieke, G. H., & Rieke, M. et al 2004, Astrophysical Journal Supplement Series, 154, 1

Zehavi, Idit, Zheng, Z., Weinberg, D. H., Frieman, J. A., & Berlind, A. A. et al. 2005, Astrophysical Journal, 630, 1

CONTACT INFORMATION

Name:	Roberto De Alba
Professional Address:	c/o Dr. Casey Papovich Department of Physics and Astronomy MS 4242 Texas A&M University College Station, TX 77843
Email Address:	robertdealba@gmail.com
Education:	B.A., Physics, Texas A&M University, May 2010 Magna Cum Laude Undergraduate Research Scholar